Biomedical Signal Processing and Control 38 (2017) 119–127

Contents lists available at ScienceDirect

Biomedical Signal Processing and Control

journal homepage: www.elsevier.com/locate/bspc

Control design for a lower-limb paediatric therapy device using linear motor technology

Farouk Chrif[a,b], Tobias Nef[b], Max Lungarella[c], Raja Dravid[c], Kenneth J. Hunt[a,*]

[a] Institute for Rehabilitation and Performance Technology, Division of Mechanical Engineering, Department of Engineering and Information Technology, Bern University of Applied Sciences, CH-3400 Burgdorf, Switzerland
[b] Gerontechnology and Rehabilitation Research Group, ARTORG Center for Biomedical Engineering Research, University of Bern, CH-3008 Bern, Switzerland
[c] Dynamic Devices AG, Technoparkstrasse 1, CH-8005 Zurich, Switzerland

ARTICLE INFO

Article history:
Received 11 October 2016
Received in revised form 17 February 2017
Accepted 16 May 2017
Available online 9 June 2017

Keywords:
Rehabilitation robots
Paediatric rehabilitation
Control systems
Impedance control

ABSTRACT

Background: Rehabilitation robots support delivery of intensive neuromuscular therapy and help patients to improve motor recovery. This paper describes the development and evaluation of control strategies for a novel lower-limb paediatric rehabilitation robot, based on linear-motor actuator technology and the leg-press exercise modality.
Methods: A functional model was designed and constructed and an overall control strategy was developed to facilitate volitional control of pedal position based on the cognitive task presented to the patient, together with automatic control of pedal forces using force feedback and impedance compensation.
Results: Each independent drive for the left and right legs can produce force up to 288 N at the user's foot. During dynamic testing, the user maintained a variable target position with root-mean-square tracking error (RMSE) of 3.8° with pure force control and 2.8° with combined force/impedance control, on a range of periodic motion of 20–80°. With impedance compensation, accuracy of force tracking was also slightly better (RMSE of 9.3 vs. 9.8 N, force/impedance vs. force control only).
Conclusions: The control strategy facilitated accurate volitional control of pedal position and, simultaneously, accurate and robust control of pedal forces. Impedance compensation showed performance benefits. Control accuracy and force magnitude are deemed appropriate for rehabilitation of children with neurological impairments, but, due to current levels required, linear motor technology may not be suitable for applications where higher force is needed. Further work is required to validate the device within the target population of impaired children and to develop appropriate patient-interface software.

1. Introduction

The recovery and maintenance of motor function is one key aim of rehabilitation interventions. Robotic technology is increasingly used in clinical rehabilitation environments to facilitate long training sessions, a large number of movement repetitions, and thereby to improve therapeutic outcomes [1].

The field of rehabilitation robotics is developing rapidly. With faster and more powerful computers, new computational approaches and sophisticated electromechanical components, robots have become an important tool to improve the therapeutic outcomes in rehabilitation [2]. Robots can aid therapists in the implementation of rehabilitation programmes by enabling repetitive, high quality task-specific movements, by increasing the duration and intensity of rehabilitation sessions and by providing a large variety of exercise modalities [3]. Furthermore, robotic systems provide the possibility of recording information about movement parameters (force, position, velocity, etc.) during exercise, which allows the subsequent interpretation and analysis of the therapy performance and progress [4,5].

The current generation of rehabilitation robots differ in terms of mechanical design, actuation technology and control architecture [1,6,7]. They can be categorized with respect to their application focus as assistive or therapeutic devices: assistive robots are used to assist patients in their daily-living activities, whereas therapeutic robots are used to improve various neurophysiological aspects of body function, and they are mainly used in clinical environments [1].

Rehabilitation robots can be further delineated with respect to their mechanical design as either end-effector or exoskeleton sys-

* Corresponding author.
E-mail address: kenneth.hunt@bfh.ch (K.J. Hunt).

http://dx.doi.org/10.1016/j.bspc.2017.05.011

Notation and abbreviations

F	measured force
F^*	target force
F_{sim}	simulated (nominal) force
F_{imp}	impedance force
θ	pedal angle
θ^*	target angle
i	current
i^*	target current
s	Laplace-transform complex variable
$C_{fb}(s)$	force feedback controller
$P_o(s)$	plant for force controller
$C_{imp}(s)$	impedance controller
C_i	current controller
P_i	plant for current controller
IPC	industrial PC

tems. End-Effector robots impose forces on the distal segments of the upper or lower limbs [8], but they cannot directly control individual joints since the contact between the patient and the robot is at limb endpoints. Examples of end-effector rehabilitation robots are the G-EO System [9], MIT-Manus [10], the Gait-Trainer [11], GENTELE/s [12] and Bi-Manu-Track [13]. Exoskeleton-based robots, on the other hand, use external structures attached at several points across the patient's limbs. The joints of the exoskeleton are aligned to those of the human body [14], which allows direct control of the joints [15]. Examples of exoskeleton robots are the Lokomat [16], LOPES [17], ARMin [18], T-WREX [19], Dampace [20] and L-Exos [21].

The dynamic leg-press form of exercise, hitherto applied mainly in the sports context for musculoskeletal conditioning [22,23], has potential as a new modality for neuromuscular rehabilitation applications. Due to the possibility of a compact design, and provision of a safe, semi- or fully-recumbent seated posture, leg-press devices have potential for application particularly in paediatric rehabilitation. Examples of leg-press rehabilitation robots are the Lambda [24], LegoPress [25] and Allegro [26].

The main aim of control strategies for leg-press devices is to provide optimal exercises to promote neuroplasticity and therefore improve motor recovery. For rehabilitation robotics in general, a variety of control strategies have been developed, and several research reviews have been done [27–30]. Rehabilitation control strategies can be categorized in two main groups: (i) trajectory tracking controllers and (ii) assist-as-needed controllers (AAN) [29]. Trajectory tracking controllers are position controllers adapted from those applied in industrial robots. They provide passive repetitive exercise, where the patient's limb is made to follow a predefined trajectory. In advanced versions, known as "adaptive position controllers", the controller allows for deviation from the predefined trajectory based on the motion of the patient [1]. Trajectory tracking controllers are important in the early rehabilitation stages, where passive exercise is needed, but lack the ability to motivate since the active participation of the patient is not of concern at this stage [30]. On the other hand, assist-as-needed controllers adjust the amount of assistance given by the robot based on the patient's real-time contribution and ability. Compared to trajectory tracking controllers, AAN controllers allow more freedom and variability of movement [31] and increase the participation and motivation of the patient [32]. One of the most appropriate AAN approaches which encourages active participation of the patient is impedance control [33,34]. Impedance control strategies allow deviation from the predefined trajectory and do not impose rigid movement. This can regulate the dynamic relationship between the motion of the patient's limb and the force applied by the actuator [35]. Furthermore, impedance control parameters can be adjusted depending on the patient's abilities and needs. Another common AAN approach is a "tunnel controller". This creates a virtual tunnel along the reference trajectory where the patient tries to maintain his limb position. As long as the limb is within the virtual tunnel, the robot will apply no corrective forces. If the limb diverges from the tunnel, the robot will increase the applied force to push the limb back to the desired trajectory [36,37]. The system described in this paper applies impedance control.

The aim of this work was to design, construct and test a novel lower-limb end-effector rehabilitation robot, based on the leg-press exercising approach, with a target population of children with neuromuscular impairments. The system which was developed, as described in this paper, is leg press training device which allows active exercise of the lower limbs. The feet are connected the footplates of two separate pedal mechanisms. The device allows movement of the lower limbs in the sagittal plane, with flexion/extension of the knee joints. The focus in the present report is on the development and evaluation of force and impedance control strategies based on linear-motor actuator technology.

2. Methods

2.1. Device specifications and design

The mechanical design and construction of the prototype device is depicted in Fig. 1 . Since the focus in the present work is on control strategy development, the mechanical design details and specifications are only summarised in brief here.

The prototype device comprises a seat with adjustable backrest and position, footplates attached via a lever mechanism to two independent linear electric motors, and a visual feedback screen positioned at the front. The patient sits on the chair with the backrest adjusted as desired between an almost upright position and an almost fully recumbent position. The feet are placed on footplates attached to separate pedal mechanisms. The maximum range of motion of the footplates is defined by the stroke of the linear motors. To adapt the robot for patients with different body sizes and leg lengths, and to give appropriate joint ranges of motion, the distance between the seat and the footplates is set by moving the chair back or forward. The visual feedback screen at the front provides the patient with motion targets and real-time feedback of key performance variables (e.g. angles and forces) for implementation of specific neuromuscular training and assessment therapies.

The target population for the device is children aged 4–14 years with body mass of up to 50 kg. The device was required to be capable of generating a total continuous force on the footplates corresponding to 1.2 × body mass, i.e. a combined left + right equivalent mass of ~60 kg. The pedals are actuated by two independent drives (left and right legs) each of which is capable of producing a continuous force of 354 N and a peak force of 1024 N. Because of the pedal geometry and available lever arms, the arrangement can generate a continuous force of 288 N at each footplate. This gives a total continuous force magnitude of 288 × 2 =576 N, corresponding to an equivalent body mass of 59 kg, which, according to the above specifications and given the ability of the motors to generate short-term forces of nearly three times the continuous levels, is deemed appropriate for therapy of children with impairments.

The therapy device was required to facilitate rehabilitation exercises for children with neuromuscular impairments. The device can be flexibly programmed for implementation of specific training exercises, and was also designed to meet the following general criteria for neuromuscular and skeletal rehabilitation [38]:

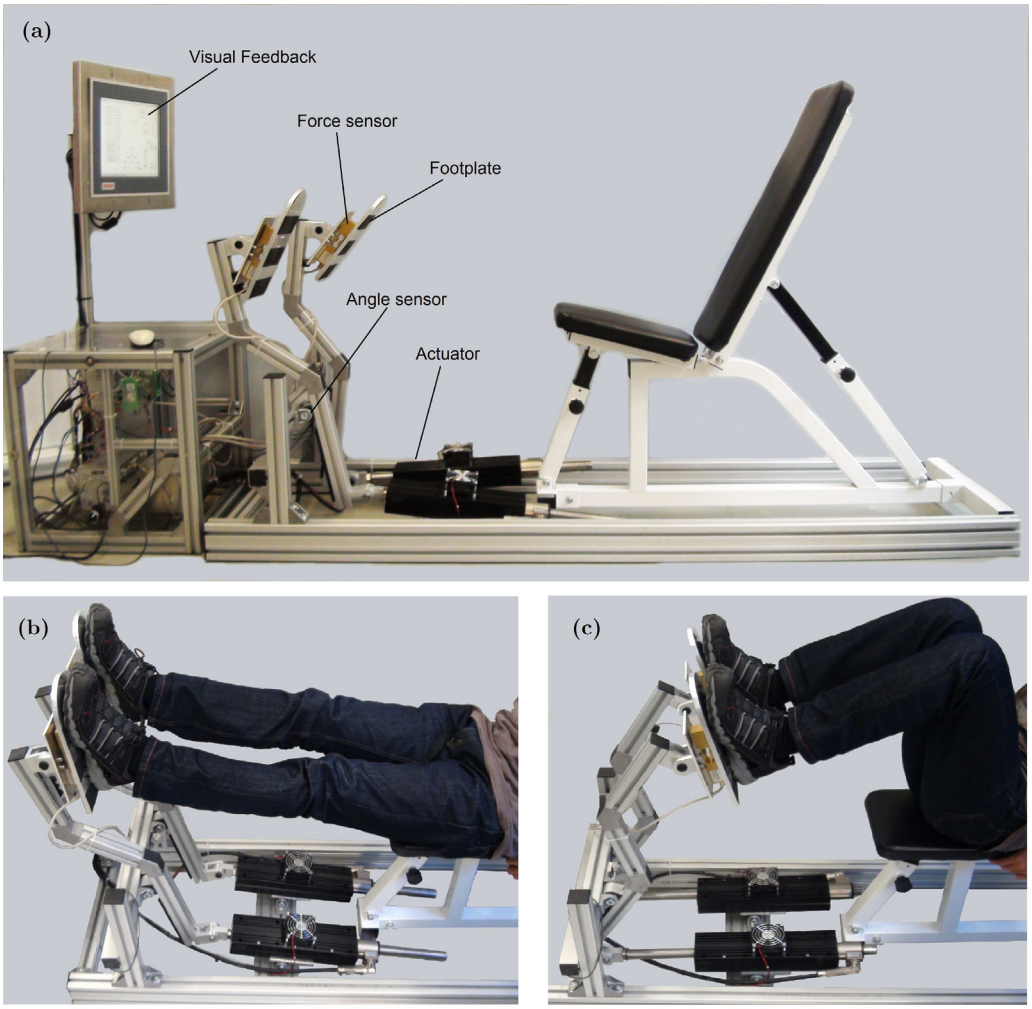

Fig. 1. Prototype of the lower-limb end-effector rehabilitation device: (a) principal components of the overall functional model; (b) detail of the linear-motor actuators. Legs at maximum extension; (c) legs at maximum flexion.

1. Flexibility and range of motion: the robot is based on bi-directional electric actuators, which allows the application of both passive and active exercises to give flexibility and arbitrary movement patterns.
2. Strength and muscle endurance: the robot is capable of providing sufficient force to improve and reinforce the patient's musculoskeletal condition, based on a multiple of maximum body mass.
3. Coordination and agility: the visual feedback module provides cognitive challenges, requires engagement of the patient and thus has potential to improve coordination using real-time, interactive sensor-controlled exercises and task-orientated training.

2.2. Overall control strategy and outcome measures

The principal task of the feedback control system is to maintain a target force F^* at each footplate, i.e. at the point of interaction between the human foot and the robot's pedal mechanism. This is implemented using a closed-loop force control system (Fig. 2), where target force $F^*(t)$ is a completely arbitrarily pre-specified profile. The left and right sides are separately controlled by independent feedback systems such that target forces for the two sides can be different: for simplicity, the control strategy is presented here as if for a single side, but in practice it is implemented in duplicate.

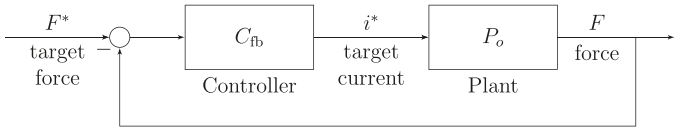

Fig. 2. Closed-loop force control system.

The feedback controller C_{fb} compares target (F^*) and measured (F) forces and continuously computes a target current i^* which is transmitted to the proprietary motor control unit; this unit, in turn, has an internal feedback controller which dynamically maintains the current actually sent to the actuator (i) close to the target i^*. The resulting motor actuation generates the force F as measured at the footplate. The overall plant to be controlled, as viewed from the controller transfer function C_{fb}, is therefore the nominal transfer function P_o linking the control signal i^* and the controlled variable F (see Eq. (3), and Fig. 2).

The basic force controller is embedded within an overall control architecture for the device, comprising also the visual feedback module (see Fig. 3). The "controller module" in the figure explicitly shows the force feedback controller and also the current controller C_i which is internal to the motor control unit (the function P_i denotes the notional plant for the current controller).

As described in the sequel (Section 2.5), the target force F^* can be augmented using an impedance controller block C_{imp} (Fig. 4);

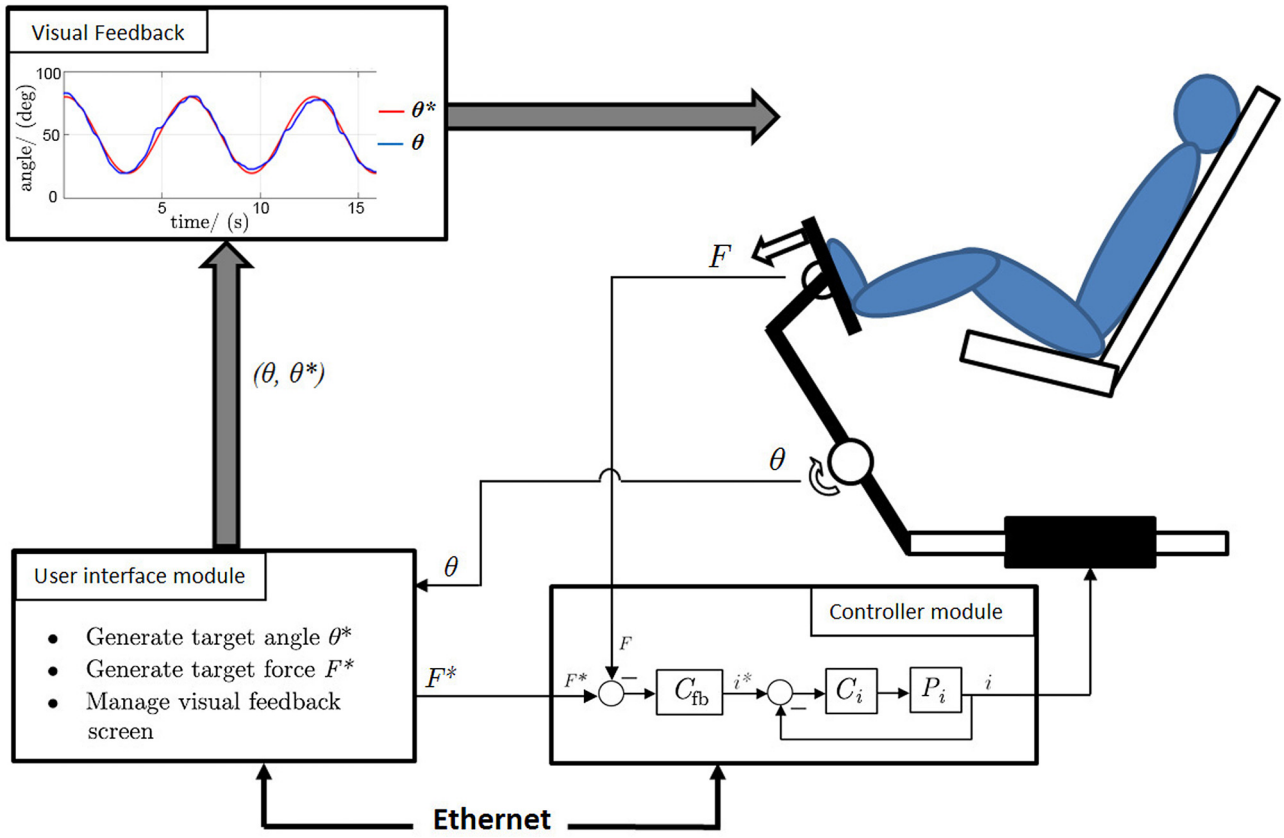

Fig. 3. Overall control architecture. The controller module regulates the forces at the footplates: it comprises a force feedback controller C_{fb} (and, optionally, an impedance control element C_{imp}, Fig. 4 and Eq. (12)), implemented within an industrial PC (IPC); the current controller C_i is embedded in a separate motor control unit. The indicated functions of the user interface module are implemented in the IPC. The nominal plant for design of C_{fb} is the transfer function from target current i^* to measured force F, $i^* \rightarrow F$: $P_o(s) = k/(\tau s + 1)$, Eq. (3) and Fig. 2 .

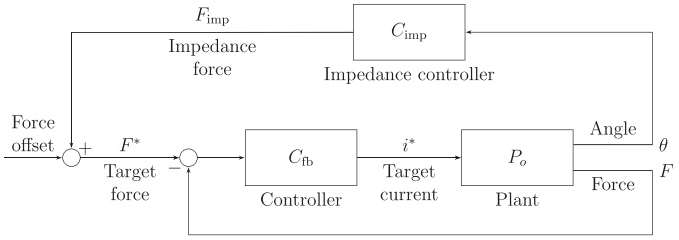

Fig. 4. Force-impedance control strategy.

this modifies the target force F^* based on position, velocity and acceleration of the pedal rotation (Eq. (12)); in this case, the variable labelled "force offset" in Fig. 4 corresponds to the target force profile F^* generated by the "user interface module" in Fig. 3 . Thus, the impedance controller C_{imp} continuously generates variations in target force in real time around the baseline profile (force offset) which is pre-specified in the user interface module. By this means, the individual components of mechanical impedance actually felt by the patient at the human-machine interaction points, i.e. stiffness, damping and inertia, can be purposely modified by setting the parameters of the C_{imp} transfer function in Eq. (12), in common with generic impedance control strategies [39].

As well as generating the target force profile F^*, the user interface module provides a movement task by means of an arbitrary target angle profile θ^*, and it manages the visual feedback screen. In its simplest form, the visual feedback displays the position target θ^* together with the actual angle θ measured by a sensor mounted at the axis of the pedal mechanism. For simplicity, in the experiments reported here for evaluation of feedback controller performance, the target angle profile was chosen as a sinusoid, while the target force was either kept constant or changed in a stepwise fashion to introduce task perturbations. For clinical applications, alternative position and force profiles should be investigated. The patient is required to keep the pedal position as close as possible to the target by means of volitional control, while the forces applied on the footplates are automatically controlled as described above. This combination of patient involvement via the cognitive position control task and the automatic force/impedance control system represents a challenging environment for neuromuscular training and rehabilitation.

Comparison of the performance of the different control strategies was based on root-mean-square tracking error (RMSE) for force and angle:

$$\mathrm{RMSE}_F = \sqrt{\frac{1}{N}\sum_{i=1}^{N}(F_{\mathrm{sim}}(i) - F(i))^2} \quad (1),$$

$$\mathrm{RMSE}_\theta = \sqrt{\frac{1}{N}\sum_{i=1}^{N}(\theta^*(i) - \theta(i))^2} \quad (2),$$

where i are the discrete time indices of the N evaluation data points and F_{sim} is the simulated nominal force. Eq. (1) gives a quantitative measure of the accuracy of automatic force tracking, while Eq. (2) measures the accuracy of human volitional control of position. Evaluation of the outcome measures was performed off-line, following real-time controller tests, using Matlab software (Mathworks Inc., USA).

Table 1
Linear motor characteristics.

LinMot P01-48x360/180x330	
Stroke	330 mm
Peak force	1024 N
Max. continuous force	354 N
Force constant	32 N/A
Max. current (@72VDC)	32 A
Max. velocity	2.1 m/s

2.3. Actuators, sensors and controller hardware

The two actuators are linear electric motors (P01-48x360/180x330, NTI AG LinMot, Switzerland). These are electromagnetic direct drives consisting of two parts: the slider, which directly provides translational motion; and the stator. The slider is a stainless steel tube filled with neodymium magnets. The stator contains the motor windings, bearings for the slider, position capture sensors and a microprocessor circuit for monitoring the motor. The linear motors are bi-directional and thus capable of generating forces in both directions. Peak force is 1024 N and the maximum continuous force is 354 N (key motor specifications: Table 1). The motors are commanded by separate control units (E1250-UC, NTI AG LinMot, Switzerland) which implement the current control function C_i indicated in the controller module (Fig. 3).

The robot has two force sensors and two angle sensors, mounted as indicated in the figure (Fig. 1(a)). The force sensors (KD140, 1 kN, Transmetra GmbH, Switzerland) are mounted behind the footplates to directly measure the forces applied by the patient. The angle sensors (GL60, Contelec AG, Switzerland) are mounted at the rotational axis of the pedals.

The force/impedance control strategy in the controller module, together with the user interface module functions (Fig. 3), were implemented in a real-time industrial PC (IPC, CX5010, Beckhoff Automation AG, Germany). The four sensor signals were interfaced directly to the IPC's analogue input channels. The IPC sends the target current commands (the control signal i^*) via Ethernet to the individual motor control units.

During real-time feedback control tests, all relevant signals (force, position) are monitored and stored using data acquisition and signal processing software (ScopeView, Beckhoff) running in the IPC. These signals are then processed off-line using Matlab as noted above. Position signals are fed back to the user in real-time as shown in Fig. 3 .

2.4. Feedback controller design

The nominal plant $P_o(s)$ linking target current and measured force was modelled as a linear first-order transfer function with steady-state gain k and time constant τ, expressed as

$$i^* \to F: \quad P_o(s) = \frac{B_o(s)}{A_o(s)} = \frac{k}{\tau s + 1} = \frac{k/\tau}{s + 1/\tau} \tag{3}$$

where the polynomials $A_o(s)$ and $B_o(s)$ are defined as $A_o(s) = s + 1/\tau$ and $B_o(s) = k/\tau$.

Model parameters k and τ were obtained empirically using step responses and system identification. During open-loop identification tests, the pedal was mechanically fixed using a rigid bar to prevent movement and step inputs were applied using the target current i^*. Eleven measurements were done with step changes in current of magnitude 2 A and 4 A, distributed across the range from 2 to 18 A. Model parameters were estimated for each measurement using linear least-squares. The gain k was found to vary between 16.1 N/A and 17.5 N/A, and the time-constant τ varied between 0.019 s and 0.026 s. Since these parameter ranges are quite narrow, the nominal model parameters were taken as the average values from the eleven measurements, giving

$$P_o(s) = \frac{16.9}{0.0226s + 1} \tag{4}.$$

The parameters of the linear compensator $C_{\text{fb}}(s)$ were obtained by following an algebraic pole-assignment approach to obtain a closed-form analytical solution, e.g. [40]. $C_{\text{fb}}(s)$ was chosen to be a linear, time invariant, strictly-proper transfer function,

$$C_{\text{fb}}(s) = \frac{G(s)}{H(s)} = \frac{g_1 s + g_0}{s(s + h_0)} \tag{5}$$

where g_0, g_1, and h_0 are real coefficients to be determined. The polynomials $G(s)$ and $H(s)$, used in the further controller derivation below, can be identified as $G(s) = g_1 s + g_0$ and $H(s) = s(s + h_0)$. By virtue of the factor $1/s$ in C_{fb}, the compensator contains integral action.

With the feedback loop of Fig. 2, the resulting characteristic polynomial of the system, denoted $\Phi(s)$, is

$$\Phi(s) = A_o(s)H(s) + B_o(s)G(s) = \left(s + \frac{1}{\tau}\right)(s + h_0)s + \frac{k}{\tau}(g_1 s + g_0) \tag{6}$$

which by expansion gives

$$\Phi(s) = s^3 + (h_0 + \frac{1}{\tau})s^2 + \frac{1}{\tau}(kg_1 + h_0)s + \frac{k}{\tau}g_0 \tag{7}.$$

The closed-loop poles are the roots of the characteristic polynomial Φ, which, from Eq. (7), has degree 3. Thus, Φ must take the structure

$$\Phi(s) = s^3 + \phi_2 s^2 + \phi_1 s + \phi_0 \tag{8}.$$

Using a pole-assignment approach, the coefficients ϕ_0, ϕ_1 and ϕ_2 are derived by arbitrary positioning of the three closed-loop poles in the s-plane. Here, the approach taken is to set one real pole at position $-a$, and to place the other two poles corresponding to the standard second-order transfer function with damping ratio ζ and natural frequency ω_n. Thus,

$$\begin{aligned} \Phi(s) &= (s + a)(s^2 + 2\zeta\omega_n s + \omega_n^2) \\ &= s^3 + (2\zeta\omega_n + a)s^2 + (\omega_n^2 + 2a\zeta\omega_n)s + a\omega_n^2 \end{aligned} \tag{9}$$

In the following, critical damping $\zeta = 1$ was employed and the parameter a was set to the open-loop pole value of $1/\tau$, i.e. $a = 1/\tau$, such that the open-loop pole was not shifted by the feedback. Further, noting that, around the critical damping value of $\zeta = 1$, ω_n is related to the 10–90 % closed-loop rise time t_r by the approximation $\omega_n = 3.35/t_r$ [41,p. 196], a single feedback design parameter, viz. t_r, was then used to obtain a desirable performance (ω_n, as required in Eq. (9), was computed as noted above as $\omega_n = 3.35/t_r$).

The unknown controller parameters g_0, g_1 and h_0 are obtained by matching coefficients of like power in Eqs. (7) and (9), resulting in

$$\begin{aligned} h_0 &= 2\zeta\omega_n + a - \frac{1}{\tau} \\ g_0 &= \frac{\tau}{k}a\omega_n^2 \\ g_1 &= \frac{\tau}{k}(\omega_n^2 + 2a\zeta\omega_n) - \frac{1}{k}(2\zeta\omega_n + a) + \frac{1}{k\tau} \end{aligned} \tag{10}$$

The experimental results described in the sequel (Section 3) were obtained using the controller tuning parameter value $t_r = 0.55$ s (desired closed-loop rise time). With the nominal plant parameters $k = 16.9$ and $\tau = 0.0226$, and with the design choices $a = 1/\tau = 44.2$ and $\zeta = 1$, the controller transfer function (5) can be calculated using the solution (10) as

$$C_{\text{fb}}(s) = \frac{g_1 s + g_0}{s(s + h_0)} = \frac{0.0543s + 2.404}{s(s + 12.73)} \tag{11}.$$

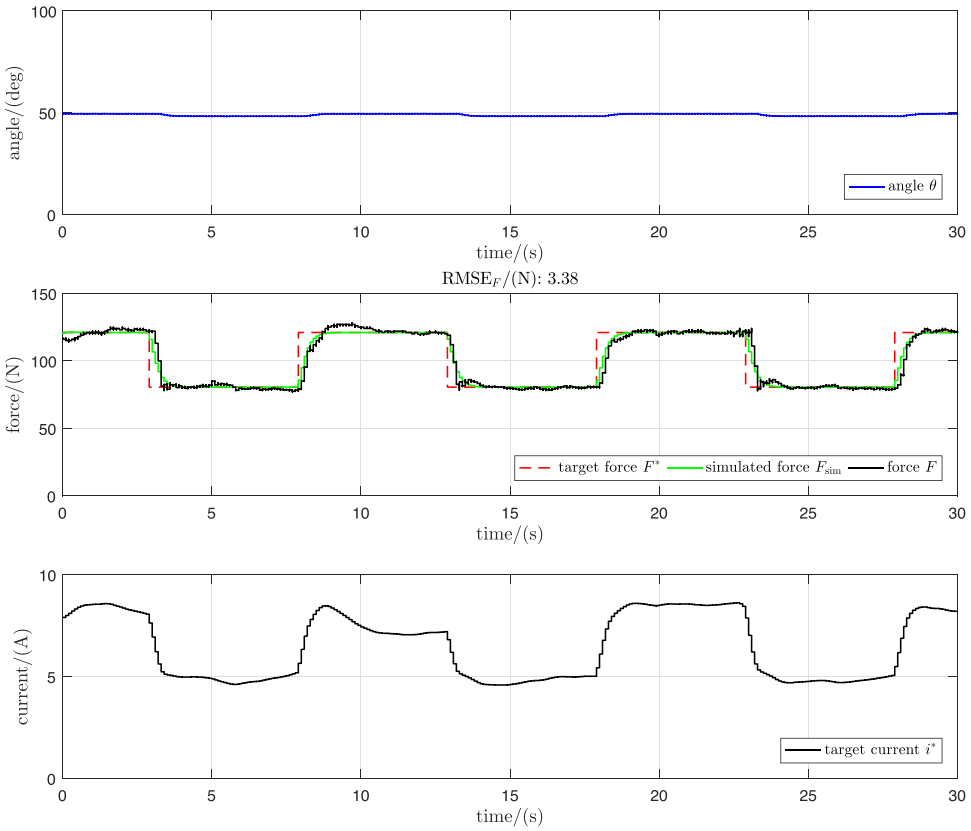

Fig. 5. Static test with pedal mechanically fixed in one position; no test person on the device.

Controllers were implemented in discrete time using a sample period $T_s = 0.05$ s.

With the design choice $a = 1/\tau$, the characteristic Eq. (6) reveals that the plant pole polynomial $A_o(s) = s + 1/\tau$ must also appear as a zero of the compensator, i.e. as a factor of $G(s)$: since A_o appears in the first term on the left of (6) and also in the right hand side (see Eq. (9), with $s + a = s + 1/\tau$), then, for a solution to exist, it must also be a factor of G in the second term of the left hand side of (6). To see that this holds in the solution of Eq. (11), G can be written as $G(s) = 0.0543(s + 44.2)$: the term $s + 44.2$ is seen to be equal to $s + 1/\tau$. This is a classical plant-pole cancellation strategy, applicable when the cancelled poles are stable and well damped [42].

2.5. Impedance controller

The impedance control strategy (Fig. 4) augments the force controller by modifying target force F^* based on angle dynamics, i.e. based on the patient's volitional movement of the pedals. The purpose is to modify the individual components of mechanical impedance perceived by the patient through the pedals.

The basic equation of the second-order dynamic relationship between the pedal angle θ and the force F_{imp} is given in the time domain by:

$$F_{\text{imp}}(t) = k_a\ddot{\theta} + k_v\dot{\theta} + k_p\theta \tag{12}$$

where k_a, k_v and k_p are the impedance parameters representing the desired modifications of inertia, damping and stiffness of the rotational system, respectively.

By Laplace transformation, the frequency-domain representation of F_{imp} is

$$F_{\text{imp}}(s) = k_a s^2\theta(s) + k_v s\theta(s) + k_p\theta(s) \tag{13}$$

and the transfer function C_{imp} is seen to be

$$C_{\text{imp}}(s) = \frac{F_{\text{imp}}(s)}{\theta(s)} = k_a s^2 + k_v s + k_p \tag{14}$$

The actual mechanical impedance given by C_{imp}, defined as the ratio of force and angular velocity, is therefore

$$\frac{F_{\text{imp}}(s)}{s\theta(s)} = k_a s + k_v + \frac{k_p}{s} \tag{15}.$$

In the results reported below, the impedance controller parameters were selected as $k_p = 0$, $k_v = 30$ and $k_a = 300$, which should serve to increase the effective damping and inertia of the system.

3. Results

Closed-loop control results are reported here for two types of test: "static" and "dynamic" tests. During the static tests, the pedal was mechanically fixed in one position (θ constant), and the response of the force feedback system to a square-wave target force F^* from 80 to 120 N was studied. This fixed-pedal configuration is the same as that used for the open-loop identification experiments (Section 2.4), and was carried out without any test person sitting on the device.

In dynamic tests, a healthy test person, using the visual feedback, was required to follow a sinusoidal target angle θ^* of frequency 0.16 Hz and amplitude of 30°. Without impedance control compensation, the target force was constant at $F^* = 90$ N. With impedance control, the force offset variable was constant at 90 N and dynamic modifications to F^* were implemented as $F^* = \text{forceoffset} + F_{\text{imp}}$ using the impedance controller parameters noted above.

The static test gave accurate force control tracking with $\text{RMSE}_F = 3.38$ N and a dynamic response close to the nominal closed-loop response with rise time of $t_r = 0.55$ s (Fig. 5 , middle graph). The

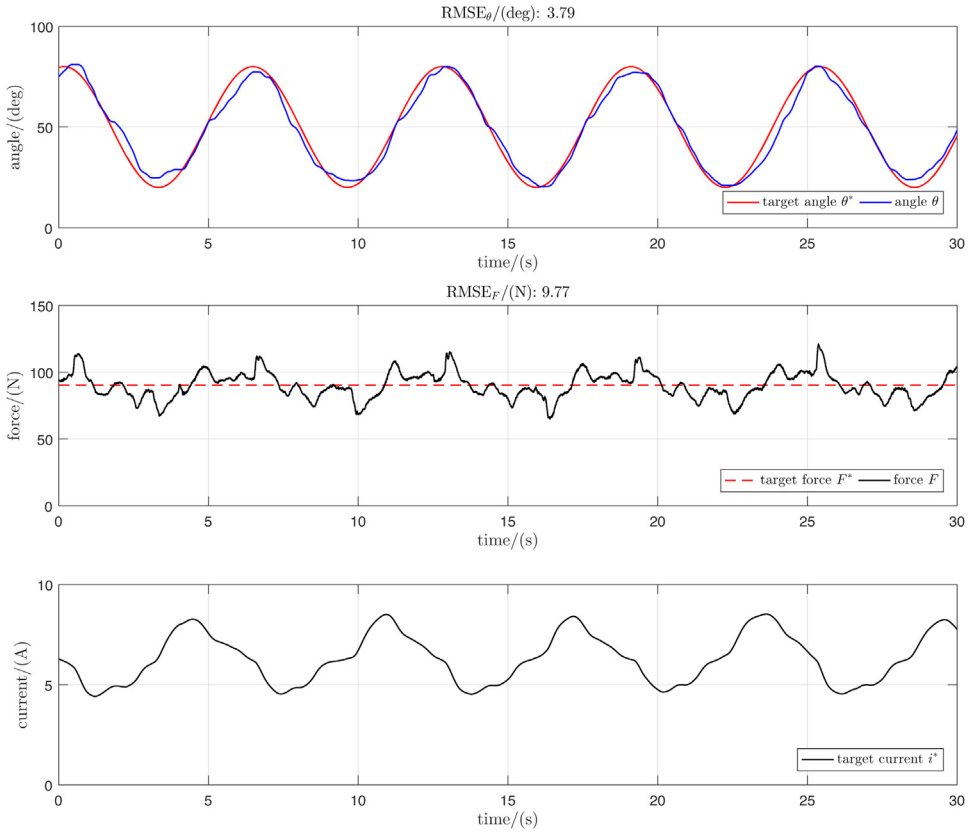

Fig. 6. Dynamic test with force controller, no impedance control. Test person volitionally follows the position/angle target profile.

control signal (target current i^*) was smooth and well behaved (Fig. 5, lower graph).

The first dynamic test reported here was carried out without impedance compensation. The test person was able to follow the target angle closely with RMSE$_\theta$ = 3.79 ° (Fig. 6, upper graph). The force controller was able, on average, to maintain the constant target force with RMSE$_F$ = 9.77 N (Fig. 6, middle graph). The measured force varied on the range of approximately 65–120 N. These values correspond, respectively, to the minimum and maximum values of the angle signal, where the user changes the direction of the movement and the magnitude of angular acceleration peaks. The target-current control signal was again smooth and well behaved (Fig. 6, lower graph).

The addition of the impedance control element resulted in improved tracking of the target angle signal with RMSE$_\theta$ = 2.82 ° (Fig. 7, upper graph; cf. no impedance, where RMSE$_\theta$ = 3.79 °). Force-tracking accuracy, with RMSE$_F$ = 9.31 N (Fig. 7, middle graph), was slightly better than the non-impedance case (RMSE$_F$ = 9.77 N). With impedance compensation, the measured force was on a substantially smaller range of approximately 71–108 N (cf. 65–120 N without impedance control); peak currents were correspondingly lower. The control signal i^* was again well behaved, albeit with a somewhat greater degree of variability when compared to the non-impedance case (Fig. 7, lower graph), due to the continuous dynamic compensation driven by changes in angular velocity and acceleration.

4. Discussion

The aim of this work was to design, construct and test a novel lower-limb end-effector rehabilitation robot, based on the leg-press exercising approach, using linear-motor actuator technology, and with a small and compact design targeted at paediatric applications. The focus here was on the development and evaluation of force and impedance control strategies.

Force controller design was based upon a simple plant model obtained as an average from multiple step tests across the operating range of the motors; these tests were performed with the pedals fixed in one position and without a test person on the device. Despite this simple and approximate approach, the feedback control performance proved to be accurate and robust across the range of conditions tested, with and without involvement of a test person.

The integration of impedance compensation gave improved target angle tracking based on volitional control by the test person, and reduced the difference between the minimum and peak forces. The mechanical design of the device had characteristics of low inertia and damping at the pedals; increasing the effective inertia and damping via the impedance compensation, resulting in turn in a lower force range, presumably modified the mechanical properties in a way that facilitated better and more accurate position control on the part of the test person.

Employment of linear motor technology contributed to the compact design characteristics and simple actuator/pedal arrangement. These features are attributable, in part, to the absence of any need for a gearing mechanism between the motors and the actuated device joints. The results, furthermore, demonstrated a high degree of motor controllability, giving accurate force control in a range suited to paediatric rehabilitation applications.

A limitation of the linear motors, and a negative consequence of the lack of gearing, is that a relatively high current is required. In the tests reported here, motor current was just over 8 A even though the measured forces were less than half of the maximum continuous force which is available. The level of force generated, and the corresponding current, is appropriate in consideration of performance specifications for therapy of children with neurologi-

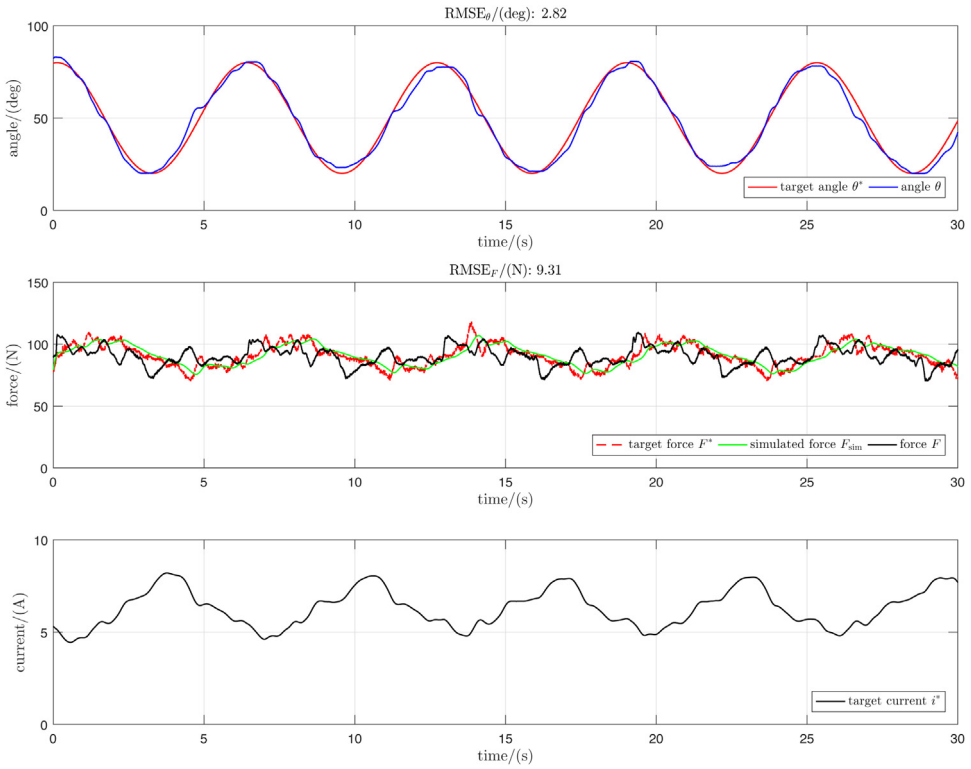

Fig. 7. Dynamic test with force controller and impedance compensation. Test person volitionally follows the position/angle target profile.

cal impairments, but scaling up to able-bodied children or to adults would be a significant limitation to the employment of linear motor technology.

5. Conclusions

The overall control strategy was found to facilitate volitional control of pedal position based on the cognitive task presented to the test person. Simultaneously, accurate and robust control of pedal forces was observed based on force feedback and impedance compensation.

The accuracy of control and the level of forces generated are deemed appropriate for rehabilitation of children with neurological impairments, but linear motor technology is unlikely to be suitable for applications where higher force levels are needed.

The next step in this work is to carry out pilot clinical evaluations to validate the prototype device within the target population of impaired children. Initial work will focus on children with impaired neuromuscular strength and coordination secondary to cerebral palsy. Performance will be evaluated using formal feasibility criteria including technical implementation, patient acceptability, and responsiveness; sample size will be determined based on a priori statistical power analysis. Further work is also necessary to develop implementations of therapy programmes and modes of operation that are task-orientated, attention-demanding and highly motivating for children, e.g. using concepts from serious games software technology [43,44]. Prior to clinical evaluation, the device design should be augmented to embody risk analysis and corresponding precautions to ensure patient safety.

Authors' contributions

All authors contributed to the study design and technical developments. FC, KJH and TN contributed to the analysis and interpretation of the experimental data. FC wrote the manuscript; KJH, TN, ML and RD revised it critically for important intellectual content. All authors read and approved the final manuscript.

Conflict of interest

The authors declare that they have no conflict of interest.

Acknowledgements

This work was supported in part by the Swiss Commission for Technology and Innovation (CTI, Grant Ref. 16081.2 PFLS-LS).

References

[1] R. Riener, Rehabilitation robotics, Found. Trends Robot. 3 (1–2) (2012) 1–137.
[2] A. Esquenazi, A. Packel, Robotic-assisted gait training and restoration, Am. J. Phys. Med. Rehab. 91 (1) (2012) 217–231.
[3] J. Robertson, N. Jarrassé, A. Roby-Brami, Rehabilitation robots: a compliment to virtual reality, in: Schedae vol. 1, Caen University Press, Caen, France, 2010, pp. 77–94.
[4] B. Rohrer, S. Fasoli, H.I. Krebs, R. Hughes, B. Volpe, W.R. Frontera, J. Stein, N. Hogan, Movement smoothness changes during stroke recovery, J. Neurosci. 22 (18) (2002) 8297–8304.
[5] J. Fang, S. Galen, A. Vuckovic, B.A. Conway, K.J. Hunt, Kinetic analysis of supine stepping for early rehabilitation of walking, J. Eng. Med. 228 (5) (2014) 456–464.
[6] M. Hillman, Rehabilitation robotics from past to present: a historical perspective, in: Z.Z. Bien, D. Stefanov (Eds.), Advances in Rehabilitation Robotics, Springer, Heidelberg, Germany, 2004, pp. 25–44.
[7] Neurorehabilitation Technology, in: V. Dietz, T. Nef, W.Z. Rymer (Eds.), Springer, London, UK, 2012.
[8] W.H. Chang, Y.-H. Kim, Robot-assisted therapy in stroke rehabilitation, J. Stroke 15 (3) (2013) 174–181.
[9] S. Hesse, A. Waldner, C. Tomelleri, Innovative gait robot for the repetitive practice of floor walking and stair climbing up and down in stroke patients, J. Neuroeng. Rehabil. 7 (30) (2010).
[10] H.I. Krebs, J.J. Palazzolo, L. Dipietro, M. Ferraro, J. Krol, K. Rannekleiv, B.T. Volpe, N. Hogan, Rehabilitation robotics: performance-based progressive robot-assisted therapy, Auton. Robot. 15 (1) (2003) 7–20.
[11] S. Hesse, D. Uhlenbrock, A mechanized gait trainer for restoration of gait, J. Rehabil. Res. Dev. 37 (6) (2000) 701–708.

[12] S. Coote, B. Murphy, W. Harwin, E. Stokes, The effect of the GENTLE/s robot-mediated therapy system on arm function after stroke, Clin. Rehabil. 22 (5) (2008) 395–405.
[13] S. Hesse, C. Werner, M. Pohl, J. Mehrholz, U. Puzich, H.I. Krebs, Mechanical arm trainer for the treatment of the severely affected arm after a stroke, Am. J. Phys. Med. Rehabil. 87 (10) (2008) 779–788.
[14] J.L. Pons, E. Rocon, A.F. Ruiz, J.C. Moreno, Upper-limb robotic rehabilitation exoskeleton: tremor suppression, in: S.S. Kommu (Ed.), Rehabilitation Robotics, Itech Education and Publishing, Vienna, Austria, 2007, pp. 453–470.
[15] H. Herr, Exoskeletons and orthoses: classification, design challenges and future directions, J. Neuroeng. Rehabil. 6 (1) (2009) 21–30.
[16] G. Colombo, M. Joerg, R. Schreier, V. Dietz, Treadmill training of paraplegic patients using a robotic orthosis, J. Rehabil. Res. Dev. 37 (6) (2000) 693–700.
[17] J. Veneman, R. Kruidhof, E. Hekman, R. Ekkelenkamp, E. Van Asseldonk, H. van der Kooij, Design and evaluation of the LOPES exoskeleton robot for interactive gait rehabilitation, IEEE Trans. Neural Syst. Rehabil. Eng. 15 (3) (2007) 379–386.
[18] T. Nef, M. Mihelj, G. Colombo, R. Riener, ARMin – robot for rehabilitation of the upper extremities, in: IEEE International Conference on Robotics and Automation, (Orlando, USA), 2006, pp. 3152–3157.
[19] R.J. Sanchez, J. Liu, S. Rao, P. Shah, R. Smith, T. Rahman, S.C. Cramer, J.E. Bobrow, D.J. Reinkensmeyer, Automating arm movement training following severe stroke: functional exercises with quantitative feedback in a gravity-reduced environment, IEEE Trans. Neural Syst. Rehabil. Eng. 14 (3) (2006) 378–389.
[20] A.H. Stienen, E.E. Hekman, F.C. Van der Helm, G.B. Prange, M.J. Jannink, A.M. Aalsma, H. Van der Kooij, Dampace: dynamic force-coordination trainer for the upper extremities, in: IEEE International Conference on Rehabilitation Robotics, Noordwijk, Netherlands, 2007, pp. 820–826.
[21] A. Frisoli, L. Borelli, A. Montagner, S. Marcheschi, C. Procopio, F. Salsedo, M. Bergamasco, M.C. Carboncini, M. Tolaini, B. Rossi, Arm rehabilitation with a robotic exoskeleleton in Virtual Reality, in: IEEE International Conference on Rehabilitation Robotics, Noordwijk, Netherlands, 2007, pp. 631–642.
[22] R.F. Escamilla, G.S. Fleisig, N. Zheng, J.E. Lander, S.W. Barrentine, J.R. Andrews, B.W. Bergemann, C.T. Moorman, Effects of technique variations on knee biomechanics during the squat and leg press, Med. Sci. Sports Exerc. 33 (9) (2001) 1552–1566.
[23] V.J. Harandi, H. Ehsani, Investigating the role of foot placement on the muscular forces of knee extensors in horizontal leg press: a static optimization approach, in: The 20th Iranian Conference on Biomedical Engineering, Tehran, Iran, 2013, pp. 59–64.
[24] M. Bouri, B. Le Gall, R. Clavel, A new concept of parallel robot for rehabilitation and fitness: the lambda, in: IEEE International Conference on Robotics and Biomimetics, Guilin, China, 2009, pp. 2503–2508.
[25] J. Olivier, M. Jeanneret, M. Bouri, H. Bleuler, The LegoPress: a rehabilitation, performance assessment and training device mechanical design and control, in: M. Auvray, C. Duriez (Eds.), Haptics: Neuroscience, Devices, Modeling, and Applications, Springer, Berlin, Germany, 2014, pp. 198–205.
[26] R. Pfeifer, F. Iida, M. Lungarella, Cognition from the bottom up: on biological inspiration, body morphology, and soft materials, Trends Cogn. Sci. 18 (8) (2014) 404–413.
[27] L. Marchal-Crespo, D.J. Reinkensmeyer, Review of control strategies for robotic movement training after neurologic injury, J. Neuroeng. Rehabil. 6 (1) (2009) 20.
[28] S. Hussain, S.Q. Xie, G. Liu, Robot assisted treadmill training: mechanisms and training strategies, Med. Eng. Phys. 33 (5) (2011) 527–533.
[29] J. Cao, S. Quan, R. Das, G.L. Zhu, Control strategies for effective robot assisted gait rehabilitation: the state of art and future prospects, Med. Eng. Phys. 36 (12) (2014) 1555–1566.
[30] W. Meng, Q. Liu, Z. Zhou, Q. Ai, B. Sheng, S. Shane, Recent development of mechanisms and control strategies for robot-assisted lower limb rehabilitation, Mechatronics 31 (2015) 132–145.
[31] S. Srivastava, P.-C. Kao, S.H. Kim, P. Stegall, D. Zanotto, J.S. Higginson, S.K. Agrawal, J.P. Scholz, Assist-as-needed robot-aided gait training improves walking function in individuals following stroke, IEEE Trans. Neural Syst. Rehabil. Eng. 23 (6) (2015) 956–963.
[32] A. Duschau-wicke, A. Caprez, R. Riener, Patient-cooperative control increases active participation of individuals with SCI during robot-aided gait training, J. Neuroeng. Rehabil. 7 (43) (2010) 1–13.
[33] H. Mehdi, O. Boubaker, Stiffness and impedance control using lyapunov theory for robot-aided rehabilitation, Int. J. Soc. Robot. 4 (1) (2012) 107–119.
[34] A.A.G. Siqueira, Impedance control of rehabilitation robots for lower limbs. Review, in: Joint Conference on Robotics: SBR-LARS Robotics Symposium and Robocontrol, Sao Paulo, Brazil, 2014, pp. 235–240.
[35] W.M. Santos, A.A.G. Siqueira, Optimal impedance control for robot-aided rehabilitation of walking based on estimation of patient behavior, in: IEEE International Conference on Biomedical Robotics and Biomechatronics, UTown, Singapore, 2016, pp. 1023–1028.
[36] A. Duschau-wicke, G.S. Member, J.V. Zitzewitz, G.S. Member, A. Caprez, L. Lünenburger, R. Riener, Path control: a method for patient-cooperative robot-aided gait rehabilitation, IEEE Trans. Neural Syst. Rehabil. Eng. 18 (1) (2010) 38–48.
[37] B. Ding, Q. Ai, Q. Liu, W. Meng, Path control of a rehabilitation robot using virtual tunnel and adaptive impedance controller, in: The 7th International Symposium on Computational Intelligence and Design, Hangzhou, China, 2014, pp. 158–161.
[38] P.A. Houglum, Therapeutic Exercises for Musculoskeletal Injuries, 3rd ed., Human Kinetics, Champaign, USA, 2010.
[39] N. Hogan, Impedance control: an approach to manipulation, J. Dyn. Syst. Meas. Control 107 (1) (1985) 1–24.
[40] K.J. Hunt, S.E. Fankhauser, Heart rate control during treadmill exercise using input-sensitivity shaping for disturbance rejection of very-low-frequency heart rate variability, Biomed. Signal Process. Control 30 (2016) 31–42.
[41] N.S. Nise, Control Systems Engineering, 3rd ed., Wiley, New York, USA, 2000.
[42] K.J. Åström, R.M. Murray, Feedback Systems, Princeton University Press, Princeton (USA)/Oxford (UK), 2008.
[43] M. Pirovano, R. Mainetti, G. Baud-Bovy, P.L. Lanzi, N.A. Borghese, Intelligent game engine for rehabilitation (IGER), in: IEEE Transactions on Computational Intelligence and AI in Games, vol. 8(1), 2016, pp. 43–55.
[44] P. Abellard, A. Abellard, Virtual reality and serious games for rehabilitation, in: International Conference on Virtual Rehabilitation, Valencia, Spain, 2015, pp. 117–118.